Nuclear Instruments and Methods in Physics Research B 344 (2015) 83–95

Contents lists available at ScienceDirect

Nuclear Instruments and Methods in Physics Research B

journal homepage: www.elsevier.com/locate/nimb

On-line implementation and first operation of the Laser Ion Source and Trap at ISOLDE/CERN

D.A. Fink [a,b,c,*,1], S.D. Richter [d,1], K. Blaum [b], R. Catherall [a], B. Crepieux [a], V.N. Fedosseev [a], A. Gottberg [a,e], T. Kron [d], B.A. Marsh [a], C. Mattolat [d], S. Raeder [d,2], R.E. Rossel [a,d,f], S. Rothe [a,d], F. Schwellnus [d], M.D. Seliverstov [a,g,h,i,j], M. Sjödin [a,3], T. Stora [a], P. Suominen [a], K.D.A. Wendt [d]

[a] CERN, 1211 Geneva 23, Switzerland
[b] Max-Planck-Institut für Kernphysik, 69117 Heidelberg, Germany
[c] Fakultät für Physik und Astronomie, Ruprecht-Karls-Universität, 69120 Heidelberg, Germany
[d] Institut für Physik, Johannes Gutenberg-Universität, 55099 Mainz, Germany
[e] Instituto de Estructura de la Materia, CSIC, 28006 Madrid, Spain
[f] Faculty of Design, Computer Science and Media, Hochschule RheinMain, 65197 Wiesbaden, Germany
[g] Petersburg Nuclear Physics Institute, NRC Kurchatov Institute, 188300 Gatchina, Russia
[h] School of Engineering and Science, University of the West of Scotland, Paisley PA1 2BE, United Kingdom
[i] Department of Physics, The University of York, York YO10 5DD, United Kingdom
[j] Scottish Universities Physics Alliance (SUPA), United Kingdom

ARTICLE INFO

Article history:
Received 6 September 2014
Received in revised form 15 November 2014
Accepted 2 December 2014
Available online 27 December 2014

Keywords:
Laser ion source
LIST
On-line mass separator
Resonance Ionization Laser Ion Source
RILIS

ABSTRACT

At radioactive ion beam facilities like ISOLDE at CERN, a high purity of the element of interest in the ion beam is essential for most experiments on exotic nuclei. Due to its unique combination of high ionization efficiency and ultimate elemental selectivity, the Resonance Ionization Laser Ion Source, RILIS, has become the most frequently used ion source at ISOLDE and at the majority of similar facilities worldwide. However, isobaric contamination predominantly stemming from unspecific surface ionization may still introduce severe limitations. By applying the highly selective resonance ionization technique inside a radio-frequency quadrupole ion guide structure, the novel approach of the Laser Ion Source and Trap, LIST, suppresses surface ionized isobaric contaminants by an electrostatic repelling potential. Following extensive feasibility studies and off-line tests, the LIST device has been adapted and refined to match the stringent operational constraints and to survive the hostile environment of the ISOLDE front-end region enclosing the highly radioactive nuclear reaction target. The LIST operation was successfully demonstrated for the first time on-line at ISOLDE during two experiments, attesting its suitability for radioactive isotope production under routine conditions. Data of these on-line characterization measurements confirm a suppression of surface-ionized isobars by more than a factor of 1000 in accordance to off-line studies that were carried out for the preparation of the on-line experiments. During the first on-line test, the suppression was associated with an efficiency loss of not more than a factor of about 50 with respect to normal RILIS operation. These losses could be further reduced to only about 20 during the second run. Results of the off-line studies in comparison to the first on-line characterization data are discussed here.

1. Introduction

The artificial production of short-lived exotic nuclei far off stability enables unique possibilities for the investigation of phenomena in various fields of fundamental as well as applied physics. To mention a few, the development of nuclear masses and ground state properties along the nuclear chart [1] are of fundamental relevance for astrophysics [2], and in particular nucleosynthesis [3], while nuclear decay properties map the stability of nuclear matter and pave the way to new physics beyond the standard model [4]; additionally, short-lived isotopes serve as ideal probes for studies on the behavior and defects in solid state physics [5] or as biomedical markers [6]. Many of the isotopes of interest have half-lives in the range of seconds or less. Low isotope production cross sections and rapid decay lead correspondingly to very low yields at on-line

* Corresponding author at: CERN, 1211 Geneva 23, Switzerland.
E-mail address: daniel.fink@cern.ch (D.A. Fink).
[1] This work contains parts of the PhD theses of D.A. Fink and S.D. Richter.
[2] Present address: Instituut voor Kern- en Stralingsfysica, KU Leuven, Celestijnenlaan 200D, 3001 Leuven, Belgium.
[3] Present address: Grand Accélérateur National d'Ions Lourds, FR-14076 Caen, France.

http://dx.doi.org/10.1016/j.nimb.2014.12.007
0168-583X/

radioactive ion beam (RIB) facilities like the Isotope Separator On-Line DEvice, ISOLDE, at CERN [7–9]. In any case, fast transport from the location of production and highest ionization efficiencies are mandatory for experiments on these species. At the ISOLDE on-line facility, radionuclei are produced by nuclear reactions in a thick target induced by bombardment with pulses of 1.4 GeV protons from the CERN PS booster. The target container is heated for fast release of the reaction products from the target material by diffusion and for rapid transport into the attached hot cavity ion source. Here the radionuclei are ionized and accelerated by high voltage for subsequent mass separation and transfer to a variety of experiments installed at the different ISOLDE beam-lines.

To produce a useful ion beam, even of the most exotic isotopes that have a low production rate, the ionization mechanism applied must be both, highly efficient and highly selective with respect to the isobaric composition of the initial reaction products. Various ion sources have been developed for this purpose to be used at ISOLDE. Their adequacy for production of a suitable ion beam of a particular radioisotope depends on the chemical properties of the element of interest with respect to those of the isobaric species that may be present [10,11]. The ion source that most closely meets these often contradictory requirements is the Resonance Ionization Laser Ion Source, RILIS. It has been in operation at ISOLDE for more than two decades providing an unrivaled combination of high efficiency and selectivity for a broad variety of elements of the periodic table [12–14]. A high-repetition rate, high power laser system provides tunable laser radiation of typically two or three wavelengths. These are precisely tuned to atomic transitions of the desired element for step-wise excitation of a valence electron and final ionization by a resonant or non resonant photo-ionization step. Excitation and ionization schemes are unique to each element and thereby ensure the high elemental selectivity of the process. Presently, ionization schemes for more than 30 elements are available at ISOLDE, while this number is steadily increasing by ongoing RILIS development work [14]. Recent applications of the RILIS include mass measurements of exotic calcium isotopes with the ISOLTRAP setup [15], the discovery of a new type of asymmetric fission in proton-rich nuclei [16], and the determination of the ionization energy of astatine [17].

The laser radiation interacts with the atoms inside a cylindrical hot cavity which is connected to the nuclear reaction target via a heated transfer line and serves as the atomizer for the diffusing reaction products. Due to the effusion from the target, a continuous flow of atoms into the hot cavity is provided and due to the radial confinement in the tube, laser ionization efficiencies of 5% to 20% are typically reached, depending on the element of choice. The atomizer cavity must be heated to about 2000 °C to prevent losses by wall sticking of the atoms, while a plasma potential, generated by thermionic electron emission from the cavity walls, provides transverse confinement of generated photo ions [18,19]. This reduces the chance of reneutrailizing wall collisions and enhances the transport and survival of the generated ions. These are pulled towards the extraction hole by the longitudinal electric field along the resistively heated cavity and by the field leakage of the extractor potential into the cavity [13].

On the other hand, the hot cavity unavoidably acts as a surface ion source for elements with low ionization energies. Thus, during RILIS operation, the ion beams produced may be significantly contaminated with surface ionized isobars. In certain cases the intensity of these surface ionized contaminants, most often stemming from alkaline or earth alkaline elements with lowest ionization energies, may exceed the intensity of the isotope of interest by several orders of magnitude and even beams of isotopes close in mass, which are not fully suppressed by the mass separator, might severely affect or even prevent experiments. One approach to reduce the ionization rate of unwanted isobaric contaminants is the use of low-work-function materials such as BaOSrO and GdB_6 for the hot cavity [20]. The drawback of this solution is the fragility of these cavities or the corresponding coatings, due to the lower operation temperatures associated with long surface sticking times and the corresponding slower response for some elements. In addition the occurrence of surface ions from other metallic structures within the target unit may appear and similarly interfere.

An alternative approach aims at spatially separating the laser ionization region from the surface ionizing environment. This is the principle of the Laser Ion Source and Trap (LIST), which has been developed by Mainz University in close collaboration with ISOLDE/CERN and the Max Planck-Institute for Nuclear Physics (MPIK) at Heidelberg [21–24].

The ISOLDE thick-target LIST is constructed as an add-on unit for the ISOLDE RILIS, incorporating a repeller electrode and a radio-frequency quadrupole (RFQ) ion guide structure as shown in the illustration of the experimental setup in Fig. 1 and in more detail in the drawing of the LIST shown in Fig. 2.

Positive ions from the hot cavity as well as from the target container and the transfer tube are completely repelled by a positive repeller potential applied to the repeller electrode and only neutral atoms are able to enter the RFQ ion guide, where the atoms of interest are selectively ionized by the RILIS lasers. The generated laser ions are confined on the axis of the LIST by a transverse RFQ potential and drift towards the extraction hole, until they experience the penetrating field of the high voltage extraction electrode. The LIST was operated on-line at ISOLDE for the first time in 2011 (*on-line run 1*) and in use for the first on-line physics experiment in 2012 (*on-line run 2*) [25].

Based on the original design concept, a similar device for hot cavity laser ion sources, the Ion Guide-Laser Ion Source, IG-LIS, was developed and recently operated on-line at the mass separator facility ISAC at the Tri University Meson Facility, TRIUMF [26,27]. At the Leuven Isotope Separator On-Line, LISOL, the LIST design for thick-target facilities such as ISOLDE and TRIUMF has been modified to couple a LIST to a gas cell catcher [28,29].

In this paper we report on the characterization and the implementation of the LIST into ISOLDE, as well as on the results of the first on-line test of a LIST device coupled to a thick-target hot-cavity ion source assembly. During the extensive preparatory testing and characterization campaigns of the LIST (LIST 1), carried out at the ISOLDE off-line separator before the initial on-line installation, laser ionization of ytterbium (Yb) and the suppression of surface ions of purposely introduced alkaline elements were demonstrated (*off-line test 1*). The LIST/target assembly and the control and data-acquisition electronics were adapted for compatibility with the ISOLDE front-end and to match the specific requirements of the operation in the target area. On-line testing under routine ISOLDE operating conditions was conducted at the front-end of the ISOLDE General Purpose Separator (GPS) using a titanium (Ti) target with the scientific goal of laser ionization of magnesium (Mg) isotopes with suppression of contamination from neighboring surface-ionizable elements. No radiation-induced degradation of performance was observed during two days of operation. A suppression of surface ions of up to 10^4 was demonstrated, at the expense of a reduction in laser ionization efficiency by a factor of approximately 50 compared to standard hot-cavity RILIS performance. Additionally, the time structure of the LIST ion pulse was measured and compared to simulations. After this successful demonstration of on-line operation, further off-line tests (*off-line test 2*) with a second newly constructed LIST (LIST 2) device were conducted for preparation of *on-line run 2*, the first on-line physics application of a LIST ion source attached to a uranium carbide (UC) target unit. This was used for the study of neutron-rich polonium [25,30]. Based on the results of the *on-line run 1*, the second

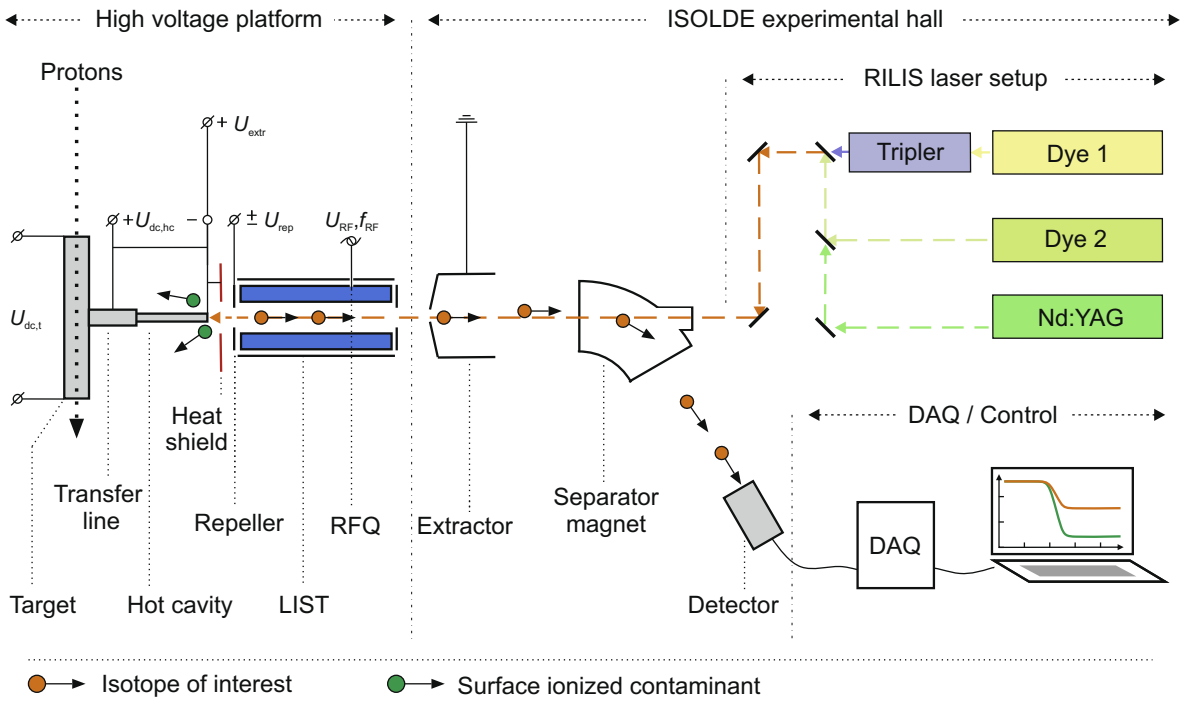

Fig. 1. Schematics of the Laser Ion Source and Trap, LIST, as installed at ISOLDE together with the laser system and the data acquisition (DAQ) and control system. Applied voltages for dc-heating of the target ($U_{dc,t}$), dc-heating of the transfer line and the hot cavity ($U_{dc,hc}$), as well as the extraction potential (U_{extr}) are indicated. LIST repeller electrode with repeller voltage U_{rep} and RFQ ion guide structure operated with RF-voltage U_{RF} and RF-frequency f_{RF} are installed immediately downstream of the RILIS hot cavity atomizer on the high voltage platform. Radiation from the RILIS lasers is sent in through a quartz window in the mass separator magnet towards the LIST and the RILIS hot cavity. Not shown: the LIST operating parameters (repeller voltage, RF-frequency and -amplitude) can be controlled remotely via glass fibers from outside the high-voltage platform by the control system. Dimensions are not to scale.

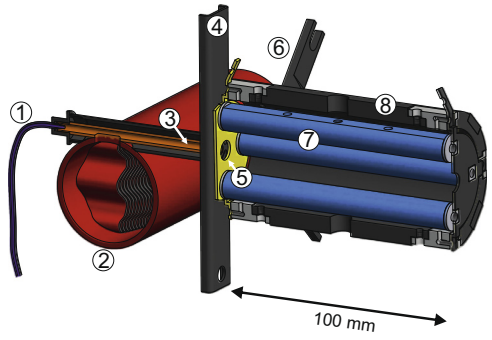

Fig. 2. Cut through the technical drawing of the Laser Ion Source and Trap device LIST and the target assembly; most important components are indicated: (1) mass marker (purple), (2) target container (red), (3) hot cavity (orange), (4) heat shield (dark gray), (5) repeller (yellow), (6) LIST holders (dark gray), (7) quadrupole rods (blue) and (8) housing (dark gray). All insulators are indicated in light gray color. (For interpretation of the references to color in this figure legend, the reader is referred to the web version of this article.)

LIST used during *on-line run 2* was slightly modified, leading to an improvement of the ionization efficiency by a factor of 2.5.

2. Experimental setup

2.1. The ISOLDE hot-cavity target

The target used for the *off-line test 1* and the *on-line run 1* (ISOLDE target #442) comprises the cylindrical, standard ISOLDE target container of dimensions length $l = 202$ mm and diameter $d = 20$ mm, filled with rolled titanium foils of 25 μm thickness as target material, a tantalum transfer line of length $l = 41$ mm and diameter $d = 5$ mm and a standard tantalum hot cavity atomizer/ionizer with dimensions of $l = 34$ mm and $d = 3$ mm as illustrated in Fig. 2. During on-line operation a driver beam intensity of 1 μA with a proton energy of 1.4 GeV was used. The target is kept on a temperature of 1500 °C while the ion source hot cavity was operated at approximately 2000 °C, both by using direct ohmic heating. The target/ion source unit was equipped with three additional, so called mass marker ovens. These consist of independently controllable, resistively heated capillaries attached to the rear end of the transfer line close to the target inlet, which were filled with samples of stable isotopes as a reference. The *off-line test 2* carried out after the *on-line run 1* used a second, widely similar LIST target/ion source unit (ISOLDE target #488). For these tests the target container was filled with SiC as a substitute for the radioactive uranium carbide, which exhibits rather similar chemical behavior and release of contaminants during heating. This target was equipped with two mass markers, filled with uncalibrated samples of ytterbium, and a mixture of rubidium (Rb) and cesium (Cs), respectively. For the *on-line run 2*, the SiC was replaced by uranium carbide for the production of neutron-rich polonium.

2.2. The Laser Ion Source and Trap

Two LIST units were used for these tests: LIST 1, installed in target #442 for *off-line test 1* and *on-line run 1*; and LIST 2, installed in target #488 for *off-line test 2* and *on-line run 2*. [4] Any dimensions of LIST 2 that differ from the LIST 1 design will be given in parenthesis below. The LIST structures were inserted into their target units 5 mm (2.5 mm) downstream the hot cavity exit hole, as shown in Fig. 1. Fig. 2 gives a cross cut through the LIST/target assembly itself. In

[4] For practical reasons LIST 2 was 1 cm shorter than LIST 1 and, to improve the laser-atom overlap inside the LIST, it was installed at a distance of 2.5 mm from the hot cavity (2.5 mm closer than LIST 1).

contrast to earlier LIST designs as set up during the development phase [23], the on-line compatible LIST design had to be significantly simplified and the number of components and potentials applied was reduced to an absolute minimum. The unit nowadays comprises two circular electrodes, which act as a repeller at the entrance and as a well-defined end electrode at the exit, both with an outer diameter of 38 mm and a central bore of diameter of 7 mm (11 mm). These are positioned at both ends of a cylindrical aluminum chamber of 100 mm (90 mm) length and 38 mm diameter. This widely closed structure shields the laser ionization region inside the LIST from any influences of the strong electric field of the extractor. Apart from small potentials applied purposely to the repeller or end electrode a longitudinally field-free region in the LIST is produced. Ions created inside the LIST will thus exhibit a narrow energy distribution and may correspondingly be extracted with low energy spread. Four rods of 98 mm (88 mm) length and 10 mm diameter are mounted parallel to the axis of the LIST cavity, equally spaced at a radius of 15 mm from the axis of the device. These rods form the RFQ ion guide structure. By application of the proper radio frequency (RF) amplitude they provide transverse confinement of ions within the LIST during their longitudinal drift towards the extraction potential. A sinusoidal RF signal with $U_{RF} = 1.2$ MHz (1.15 MHz) frequency and up to $U_{RF} = 500\ V_{pp}$ amplitude is applied to the rods. The signal is reversed between adjacent rods to generate the radial quadrupole potential. In the present realization the LIST device uses just the RF potential at the four quadrupole rods and a single DC potential at the repeller electrode of up to $U_{rep} = \pm 500$. The effect of an additional DC potential at the extractor was tested during *off-line test 1*, but no improvement of the ionization efficiency was observed for a negative bias. The tests suggest that the extraction field that is penetrating through the extraction electrode is sufficient for efficient extraction of the ions from the LIST cavity. In order to reduce the complexity of the setup, the DC potential at the extractor was therefore removed for the on-line run 1 and all experiments thereafter. Correspondingly, only two vacuum feedthroughs for symmetrically introducing the RF potentials and an additional one for the DC repeller voltage had to be provided supplementarily at the LIST target/ion source unit. However, a possible effect of a DC potential on the extraction electrode and the LIST housing to the energy spread and the emittance could be subject of future experiments and simulations.

Laser ionization will take place wherever there is a suitable overlap between the cloud of effusing atoms and the laser radiation. This includes the volumes inside the transfer line, the hot cavity, and finally along the central axis of the LIST structure.

The setting of the repeller voltage and its polarity determines the mode of operation of the LIST:

Ion guide mode:
The ion beam comprises ions that were produced in the hot cavity and along the longitudinal axis of the LIST. A negative repeller voltage enables and even enhances passage of hot cavity ions. The LIST RFQ operates as an ion guide for transport of the ions to the extraction field that is penetrating through the extraction aperture into the LIST.

LIST mode:
A suitable positive voltage repels all ions that are created inside the transfer line and the hot cavity by surface ionization or laser ionization so that only neutral atoms enter the LIST. Only the fraction of ions that were laser ionized inside the LIST reach the ISOLDE beam line.

2.3. The ISOLDE off-line mass separator setup

The ISOLDE facility at CERN provides a dedicated off-line mass separator facility for development, conditioning and testing of target/ion source units, which is described e.g. in [20]. The front-end geometry and the ion optical elements closely match those of both, the ISOLDE GPS (General Purpose Separator) and HRS (High Resolution Separator) front-ends, to allow for direct installation of standard ISOLDE target/ion source units. Beams of stable isotopes are extracted with up to 60 keV ion energy, mass analyzed in a 60° sector field magnet and can be detected using either a Faraday cup (FC) or a micro-channel plate (MCP). For testing the LIST performance, the corresponding target units prepared for subsequent on-line installation, were installed there first. Mass marker fillings of ytterbium, cesium (Cs) and rubidium (Rb) were used to dispense laser and/or surface ionizable species as required. For resonance ionization, a Nd:YAG laser pumped system consisting of two RILIS Ti:Sa lasers (Mainz University design) [31], operating at 10 kHz repetition rate, was installed close to the separator magnet. The Ti:Sa lasers were initially tuned to the ionization scheme for ytterbium, as shown in Fig. 3, involving frequency tripling of one of the lasers. The set of measurements, as performed with this arrangement off-line, included transmission studies through the LIST in both, *ion guide*- and *LIST mode* by application of so-called repeller scans; investigations on the achievable selectivity, and the determination of the overall ionization efficiency in both modes using calibrated amounts of sample material in the mass markers.

2.4. On-line implementation of the LIST at ISOLDE

For on-line operation of the LIST at the ISOLDE front-end several specific technical requirements had to be met:

(i) *High radiation level.*
The LIST has to endure the harsh conditions at the target front-end. Reliable operation in a permanent radioactive level of up to 1 kGy/h in the direct vicinity of the target and in a high-temperature environment of > 1500 °C must be ensured routinely for many days to weeks. After irradiation with protons, the target unit remains highly activated and inaccessible for any handling or inspection. No error analysis, maintenance or repair is possible in the event of a failure of a LIST component. Correspondingly, all electrically insulating components of the LIST are manufactured from radiation hard and temperature resistant materials (Boron Nitride (BN) or PolyEther Ether Ketone (PEEK)) and total quality management of the assembly procedures was attempted as a protective measure.

(ii) *Transport of electrical potentials and signals to the LIST target/ion source unit.*
Due to the extended concrete shielding enclosure of the ISOLDE target area, the RF-signals and the repeller voltage had to be applied via about 20 m long cables which connect the power supplies located in the high-voltage (HV) cage outside the shielding to the high-voltage platform of the front-end through a long insulator tube. For low loss transmittance of the RF signal an impedance matched cable was used. The sinusoidal RF signal is transmitted as a single-line, low voltage ($V_{eff} < 50$ V) signal from the amplifier mounted in the external HV cage to a transducer box attached to the LIST target to minimize high-frequency radiation losses along the cable at the frequencies around 1 MHz and corresponding signal distortion. A photograph of the complete LIST/target assembly for the *on-line run 1* including the transducer box is shown in Fig. 4. This box is a genuine part of the LIST target/ion source unit, being mounted about 50 cm above the ISOLDE target/ion source container. It houses an inductor-capacitor (LC) circuitry, which converts the single line, low voltage RF-signal into a symmetric volt-

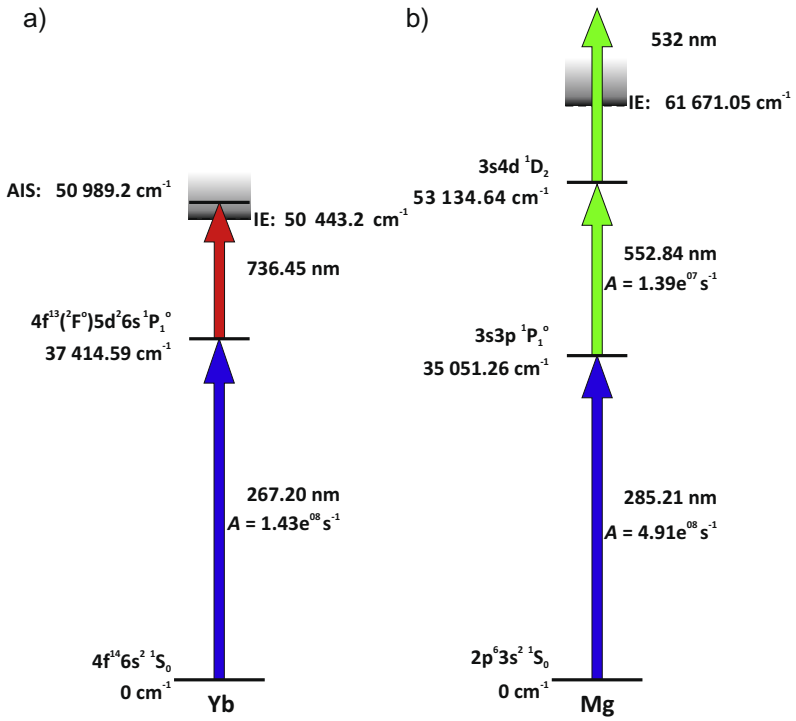

Fig. 3. Laser ionization schemes for ytterbium (Yb) and magnesium (Mg) as used in the experiments.

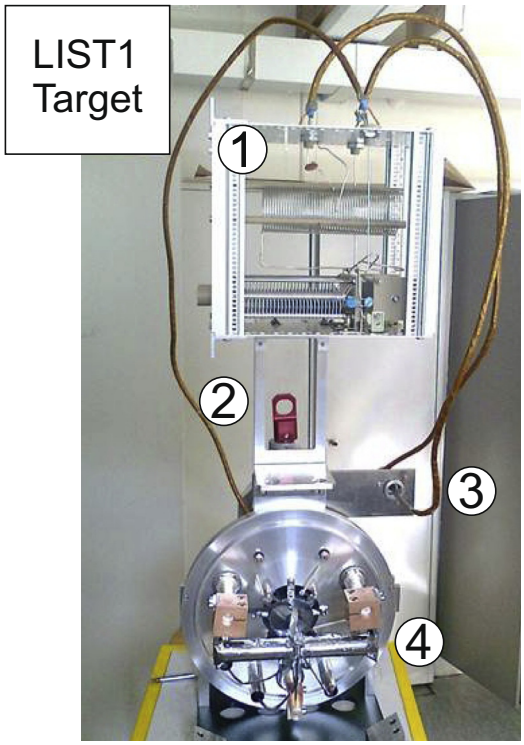

Fig. 4. LIST 1 target before the installation into ISOLDE for *on-line run 1*: The main components are: (1) transducer box, (2) support for transducer box, (3) RF-connector, and (4) opened target.

age of up to $U_{RF} = \pm 500 V_{pp}$, which is applied to the quadrupole rods of the LIST RFQ via two low-loss electrical vacuum feedthroughs. This arrangement ensures minimum signal degradation and power loss along the transfer cable length.

(iii) *Handling and coupling of the LIST target by the ISOLDE front-end robot.*
To ensure reliable remote handling and coupling of the LIST target to and from the ISOLDE GPS front-end by the ISOLDE industry robot, a specially designed mount for the transducer box at the target unit and a corresponding plug connector for the RF line was installed at the LIST target/ion source unit as shown in Fig. 4. This allows for secure automatic coupling of the complete unit to the GPS front-end in a way to not restrict the robot movements or to alter the center of gravity of the assembly.

(iv) *Remote control of LIST parameter settings and data acquisition.*
Access to the electronic equipment in the HV-cage is impossible during ISOLDE operation. Power supplies for RF and repeller voltage were thus equipped with input connections via glass fibers, which allow for the remote control of these electronic units. A LabVIEW based LIST control system was developed and integrated into the RILIS control system [32].

2.5. On-line setups in use

During the *on-line run 1* the conventional RILIS laser system was used. The wavelength was tuned to the ionization scheme for magnesium, as shown in Fig. 3. The setup consisted of two *Sirah Credo* dye lasers that were delivering radiation to drive the first two resonant transitions and part of the 532 nm output of the pump laser (frequency doubled *Edgewave* Nd:YAG) was used for the non-resonant ionization step. One of the dye lasers was frequency-doubled to provide the necessary UV-photons for the first excitation step. More details of the RILIS laser system are found e.g. in [14]. Before the installation at the GPS front-end, this target/ion source unit was prepared with an uncalibrated magnesium sample in one mass marker for initial testing and optimization and one calibrated magnesium mass marker of $2.4 \cdot 10^{16}$ atoms for an ionization efficiency measurement. All extracted ion beam intensities above 0.1 pA were measured with the ISOLDE Faraday cups. For less

intense beams of radioactive isotopes, the yields were determined using the ISOLDE tape-station, which is equipped with sensitive β- and γ-detectors.

For the *on-line run 2*, the RILIS lasers were tuned to magnesium for the setup and testing procedure in the beginning and for comparison with the *on-line run 1* and were then configured for the ionization of polonium, including a tunable, bandwidth-reduced Ti:Sa laser for laser spectroscopy purpose. The radioactive magnesium ions were detected by the ISOLDE tape-station and the polonium ions were detected with the KU Leuven Windmill setup for the detection of α-emitters [33]. For more details of the setup of *on-line run 2*, we refer to our other publications [25,30].

3. Experimental results

3.1. Quantification of selectivity and efficiency of the LIST

The performance of the LIST can be characterized by a limited number of parameters: the *laser ionization efficiency* ϵ, the *selectivity S*, the *LIST suppression factor LSS*, and the *LIST efficiency loss factor LLF*.

The ionization efficiency ϵ of an ion source is defined in general as

$$\epsilon = \frac{\text{Number of ions emitted from the source}}{\text{Total number of atoms in the initial sample}}. \quad (1)$$

This quantity is most reliably determined by measuring and integrating the ion current during the entire evaporation of a carefully calibrated sample of the element of interest. Unfortunately, this type of absolute efficiency measurement is both, time consuming and error prone, and may not be applied under on-line conditions. Somewhat less expressive but very simple and more practical is the approach to access the relative LIST efficiency by comparing the *LIST mode* and *ion guide* ion currents. Since the LIST implies laser ionization outside the confinement of a hot-cavity, a significant reduction in efficiency is unavoidable. In addition, it is expected that laser ionization inside the hot-cavity also contributes to the loss factor since a small fraction of atoms corresponding to the RILIS laser ionization efficiency is already laser ionized inside the hot cavity before reaching the RFQ and are thus repelled by the repeller voltage together with the contaminants. These effects lead to the total *LIST loss factor* in efficiency, *LLF*, which is defined as

$$LLF = \frac{\text{Laser ion intensity in } \textit{ion guide mode}}{\text{Laser ion intensity in } \textit{LIST mode}}. \quad (2)$$

The selectivity S in an ion beam experiment can be defined as

$$S = \frac{\text{Ion intensity of the isotope of interest}}{\text{Ion intensity of contaminants for similar conditions}}. \quad (3)$$

Unfortunately, the quantity of the selectivity can not be determined easily in most cases. Its value may even furthermore depend on the specific origin of the contaminants, i.e. atomic or molecular isobars, contributions from neighboring masses or unspecific background from radioactivity or electronics. Correspondingly, isotopic, isobaric or overall selectivity may in principle be defined separately, while individual contribution are usually not distinguishable in the experiment. The primary goal of the LIST is the increase of the selectivity by removal of surface ionized contaminants from the ion beam by the repeller voltage (*LIST mode*). The strength of this suppression in *LIST mode* relative to *ion guide mode* is given by the LIST suppression factor *LSF*

$$LSF = \frac{\text{Ion intensity of contaminant in } \textit{ion guide mode}}{\text{Ion intensity of contaminant in } \textit{LIST mode}}. \quad (4)$$

3.2. Modes of LIST operation

There are only two parameters which determine the mode and optimum operation of the LIST:

(i) the amplitude of the RF voltage, which is chosen according to the mass of the element of choice and
(ii) the repeller voltage, which must be separately optimized for choosing either the selective *LIST mode* or alternatively the highly efficient but significantly less selective *ion guide mode* (IG mode).

3.3. Setting of the proper RF potential

The influence of the amplitude of the RF voltage on the performance of the LIST in both, *LIST* or *ion guide mode*, has been investigated and optimized during the whole set of off-line and on-line measurements. Final results were obtained during the *off-line test 2* at the ISOLDE off-line mass separator. Transmission through the LIST RFQ ion guide was studied as a function of the applied RF-potential for various isotopes along the mass range of 23 to 174 u. A negative repeller potential of -50 V was applied in *ion guide mode* for the extraction of surface ions of sodium (Na), calcium (Ca), rubidium (Rb) and cesium (Cs) from the hot cavity. Comparison between *LIST* and *ion guide mode* was made by using laser ionized ytterbium, for which the repeller voltage was set to $U_{rep} = +7$ V and $U_{rep} = -100$ V, respectively. Fig. 5 shows the ion current as a function of the RF amplitude for all species mentioned. The ion current measurements were normalized to the maximum ion current that was recorded for each isotope. In the left figure, the LIST transmission in *ion guide mode* is shown. According to the stability diagram for a non-ideal quadrupole structure of finite length, operated in RF-only mode [34], the curves exhibit a mass dependent, characteristic shape: starting from low RF potential a steep increase leads to a mass dependent optimum transmission followed by a slow decrease until the upper end of the first stability range is reached (visible e.g. for ^{23}Na at $U_{RF} \approx 380\,V_{pp}$). As expected, the optimal RF amplitude is higher for higher masses, while a strict proportionality, as predicted by theory, is not observed. This discrepancy is attributed to influences of the fringing field at the entrance, which affects transmission curves of the different elements differently.

The right graph in Fig. 5 compares the transmission of laser ions, i.e. laser ionized ^{174}Yb, in *ion guide mode* ($U_{rep} = -100$ V) and in *LIST mode* ($U_{rep} = +7$ V). In *ion guide mode* the ion current develops rather identical to the behavior of the surface ionized elements. It peaks for an RF-signal of about 150 V and decreases for a further increase of the RF amplitude. The rather large RF value at the maximum value is related to the significantly higher repeller voltage of ($U_{rep} = -100$ V) and the interference of this electric field. In contrast, for the *LIST mode* the ion current of ytterbium reaches its maximum already at a much lower RF amplitude of less than 100 V and remains almost constant for any further increase of the RF amplitude up to the maximum of $U_{RF} = 400\,V_{pp}$. This severely different behavior is ascribed to the very different location and initial conditions of ionization. In *LIST mode* laser ions are generated in a well-defined cylindrical volume with diameter of ≈ 3 mm along the RFQ axis. Apart from the avoidance of the fringe field before the RFQ entrance, the atoms thus have very low transverse kinetic energy and, correspondingly, interact only with the innermost part of the quadrupole potential. In addition they experience only a reduced quadrupole length depending on their point of formation. As a final discrepancy to the ion guide mode, the repeller voltage in LIST mode is only $U_{rep} = +7$ V and interferes much less with the quadrupole potential of the LIST. As has been verified qualitatively by simulation, these factors lead to a stability

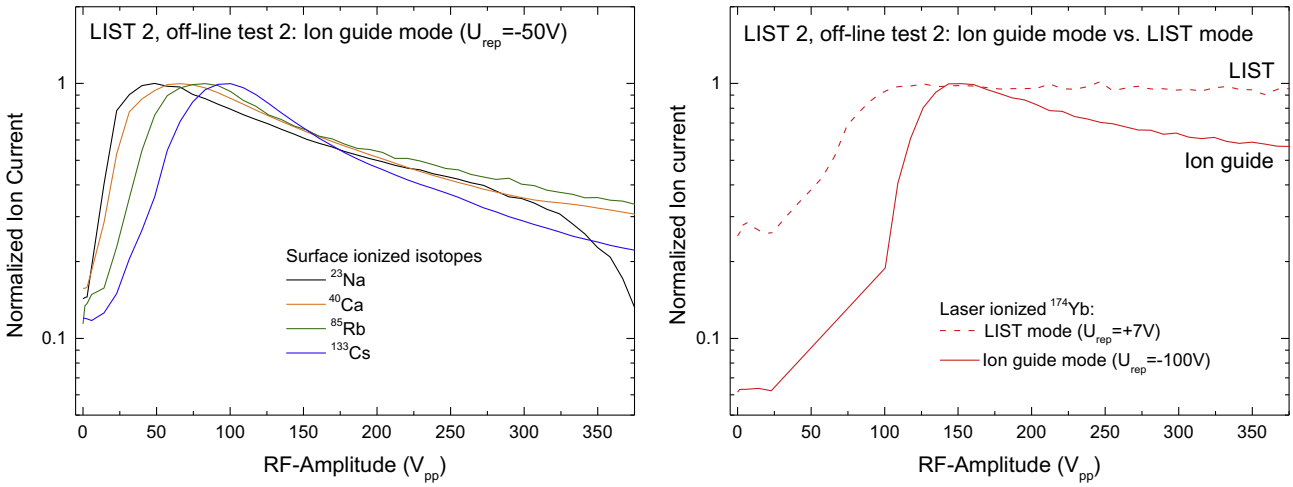

Fig. 5. Measurements of the ion transmission through the LIST RFQ ion guide conducted at the ISOLDE off-line separator with LIST 2 during *off-line test 2*. For each species, the ion current is normalized to the maximum ion current that was measured and is given as a function of the RF voltage applied to the rods of the RFQ ion guide. Left: surface ionized ^{23}Na, ^{40}Ca, ^{84}Rb and ^{133}Cs ions in ion guide mode ($U_{rep} = -50$ V). Right: laser ionized ^{174}Yb in LIST mode ($U_{rep} = +7$ V) compared to ion guide mode ($U_{rep} = -100$ V).

range, which is significantly extended towards lower as well as higher RF potentials in comparison to the situation of the ion guide mode. The selection of the amplitude of the RF voltage thus is not critical in a wide range for the preferable operation of the LIST in *LIST mode*, while *ion guide mode* operation does require proper adaptation depending on the mass range of interest.

3.4. Switching between LIST and ion guide mode

The highly selective *LIST mode* can be set by applying a range of positive repeller voltages, for which the suppression of surface ionized ions is highest, while *ion guide mode* is chosen by applying repeller voltages, for which the intensity of the laser ionized isotope of interest is highest. Corresponding optimization was carried out by scanning the repeller voltage in a wide range of −220 to +220 V. A typical result from *off-line test 1* with LIST 1 is illustrated in Fig. 6. Here, the repeller scan gives ion currents of both, laser and surface ionized ^{174}Yb, as a function of the repeller voltage. The ion current has a rather flat, extended maximum in the range of negative repeller voltages peaking at −55 V to −25 V, which corresponds to optimum *ion guide mode*. Ideal *LIST mode* repeller voltage is reached when the surface ionized ytterbium ion current is fully suppressed, i.e. falls below the detection limit of the Faraday cup. This is the case above $U_{rep} = +5$ V with a rather constant trend for positive voltages above that value. A very minor increase in the ion currents, which is observed from around $U_{rep} = +25$ V to +60 V, is ascribed to electron impact ionization by electrons emitted from the tantalum surface of the hot cavity. The slight decrease of the laser ion source current in LIST mode for growing positive repeller potential is caused by disturbances and defocussing effects of the repeller potential at the laser ionization region close to the electrode. Optimum LIST operation is thus obtained at repeller voltages of $U_{rep} = +7$ V to +12 V. The corresponding two voltage regions for *LIST* or *ion guide mode* are indicated in Fig. 6 as hatched regions.

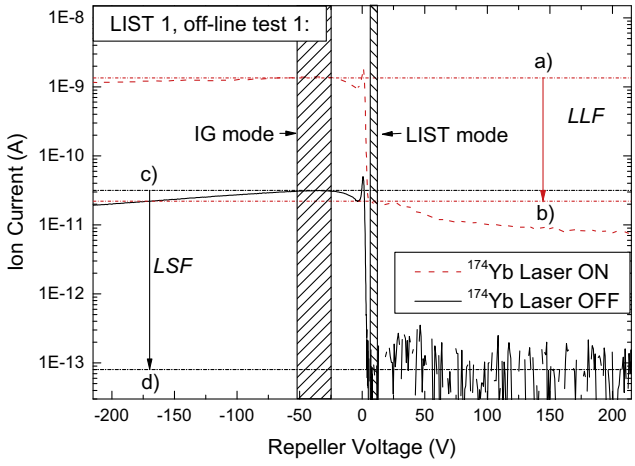

Fig. 6. Ion current of laser ions (dashed red line, laser on) and surface ions (solid black line, laser off) of ^{174}Yb as a function of the repeller voltage, measured at the ISOLDE off-line separator during the *off-line test 1* with LIST 1. The regions of ion guide (IG) and LIST operation are indicated as hatched fields. The definitions of the LIST efficiency loss factor *LLF* and the LIST suppression factor *LSF* are illustrated in the figure: *LLF* is the ratio of the ion current in *ion guide mode* (a) and the ion current in *LIST mode* (b); *LSF* is the ratio of the ion current in *ion guide mode* (IG mode) (c) and the ion current in *LIST mode* (d). The latter is limited by the Faraday cup readout noise. (For interpretation of the references to color in this figure legend, the reader is referred to the web version of this article.)

3.5. Time structure of the LIST ion pulse

The time structure of the laser ionized ion bunch from the LIST was studied on ^{24}Mg during the *on-line run 1* at ISOLDE. The ion arrival time was recorded at the micro-channel plate (MCP) detector with respect to the laser pulse timing. The MCP was located approximately 20 m downstream in the ISOLDE beam line. Data was taken for three different settings of the repeller voltage ($U_{rep} = +7$ V, $+10$ V and $+40$ V), as shown in Fig. 7. For each time scan, the observed ion bunch structure is comprised of three individual components, labeled (A) to (C) in the figure, i.e. two separate rather short peaks (A) and (B) and an extended tail (C) of peak (B) that shows a repeller voltage dependent substructure. An attempt was made to reproduce these structures and dependencies using a mathematical model. The time-independent longitudinal potential distribution inside the LIST was simulated with the commercial software package *Charged Particle Optics*© (CPO©), taking into account the penetrating potential of the ISOLDE extraction electrode. CPO is a software for the accurate simulation of electrostatic potentials of ion optical elements using the *Boundary Element Method* [35]. For subsequent calculation of the ion flight times, the potentials inside the LIST were approximated by empirical func-

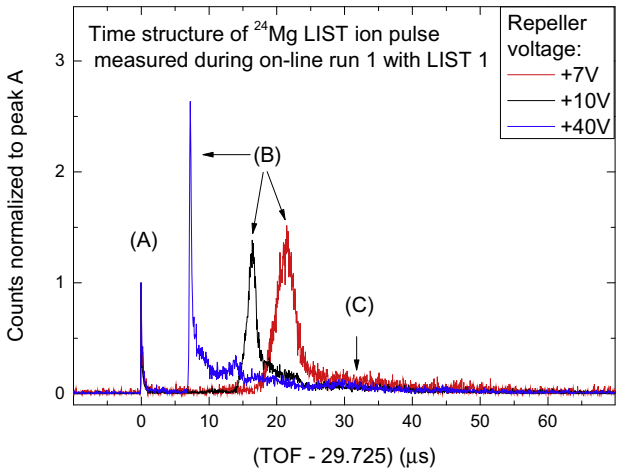

Fig. 7. Time structure of laser ionized ^{24}Mg for repeller voltages of $U_{rep} = +7$ V, $+10$ V and $+40$ V measured with LIST 1 during *on-line run 1*. The time of flight (TOF) is given with respect to the first peak (peak A) in the spectrum at $t = 29.725$ µs, which corresponds to the time of flight through the mass separator to the experiments. The ion counts of each spectrum are normalized to peak (A). In addition to peak (A), a second, more intense peak (B), whose time and strength varies with the repeller voltage, and a rather broad structure (C) can be identified.

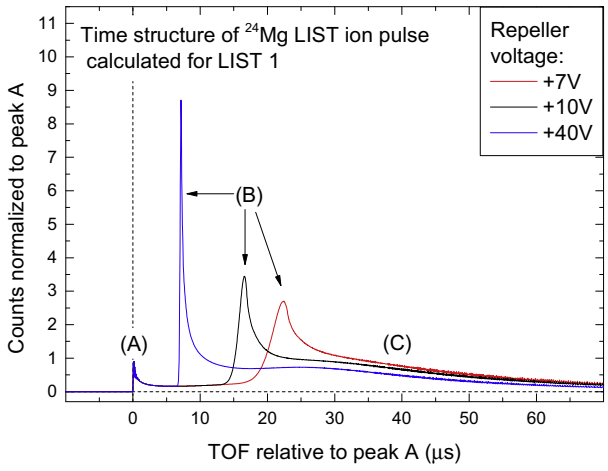

Fig. 8. Simulated LIST 1 time structure for $U_{rep} = 7$ V, 10 V and 40 V. The time of flight (TOF) is given with respect to peak (A) and the count rate is normalized to peak (A).

tions. The effusing atomic beam was inserted in a simple model with a divergence of a constant angle. This leads to an atom density that is inversely proportional to the square of the distance from the repeller electrode. The time of flight was then calculated for a set of initial starting positions and velocities, weighted by the Maxwell velocity distribution n for a hot ion source cavity temperature of $T = 2000$ °C. Fig. 8 shows the resulting calculated time structure for the identical repeller voltages $U_{rep} = 7$ V,10 V and 40 V.

Almost surpassing the expectations, this simple simulation reproduces all three main features, peak (A), peak (B) and tail (C) of the measured time structure well; in particular the dependence of the positions and the widths of the individual peaks (B) on the repeller voltage agree very well with the measured values. The relative intensities of the measured and the simulated peaks agree less well. In particular, the propagation of the tails (C) is overestimated, which might be explained by the fact, that in this simplified model, the acceptance of the RFQ or any angular preference of the laser ionization process is not considered. The calculated dependence of the intensity of peak (B) for increasing repeller voltages seems realistic, while the experimentally observed deviation from this trend for $U_{rep} = 7$ V could have been induced by some instabilities in the ion source during the measurement. Obviously, also the weak substructure observed in the tail (C) was not reproduced, but may be explained by the influence of the RF-potential that was not considered in the simulations. Nevertheless, the simulated time structures allows for the explanation of the three dominant components, (A)–(C) as follows:

Peak (A) appears after the minimum flight time of ≈ 30 µs and is unaffected by a change in repeller voltage. It is attributed to ions that are created very close to the exit of the LIST. Here, the strong potential of the extraction electrode penetrates into the LIST cavity and produces a sharp time focus. It contains only very few ions, as the origin is far from the ion source hot cavity exit hole.

Peak (B) This most intense peak of the time structure shows an intensity and temporal appearance that is strongly dependent on the repeller voltage. It is attributed to ions created close to the repeller electrode, i.e. within the extension of the repeller field, where the atom flux density is highest. The time of flight crucially depends on the repeller potential defining the ion energy during their drift along the LIST axis, while the peak widths represents the initial energy distribution of the ions.

Tail (C) For those ions created along the entire length and in particular at the central part of the LIST RFQ structure, the ion arrival time is affected by the individual position of origin of the ion and the phase of the Rf field. In addition the initial thermal velocity of the atom plays a more vital role. Correspondingly this component, i.e. the tail of peak (B) is not at all symmetrical, broader and even shows some substructuring by the RF frequency.

As expected, inside the LIST, the majority of the ions are created close to the repeller electrode, where the atom beam density is the highest. This is visible in the integrated area of peak (B), which is specifically large for low repeller voltage settings. In the case of the experimentally determined time structure shown in Fig. 7, peak (B) accounts for more than 60% of the ion signal. This is more than was calculated for peak (B) in the simulations, where the ions were distributed equally between peak (B) and tail (C). The more intense and broader structure of the simulated tail (C) implies that the atom density far from the repeller is over-estimated by the model.

As a consequence a further gain in efficiency in *LIST mode* was expected by minimizing the gap between the hot cavity exit and the repeller electrode from 5 mm during *on-line run 1* to lower values in order to increase the atom density behind the repeller potential barrier. This could in fact be demonstrated during the *on-line run 2* with the slightly modified LIST 2 [25] setup, where the distance of the LIST quadrupole structure to the hot cavity exit was reduced to 2.5 mm. As a result, the *LIST mode* ionization efficiency was increased by a factor of 2.5, corresponding to an improved *LLF* = 20 for LIST 2.

3.6. Selectivity

In the repeller scan of Fig. 6, surface ionized ^{174}Yb is suppressed in *LIST mode* to the Faraday cup detection limit. This prevents the accurate evaluation of the LIST suppression factor in this case.

Fig. 9 shows wide range mass scans of surface ionized isotopes – with lasers turned off – in the mass range from 20 u to 75 u and from 125 u to 180 u measured at the off-line separator with LIST 2 during the *off-line test 2*. In *ion guide mode*, ^{23}Na, ^{27}Al, ^{39,41}K,

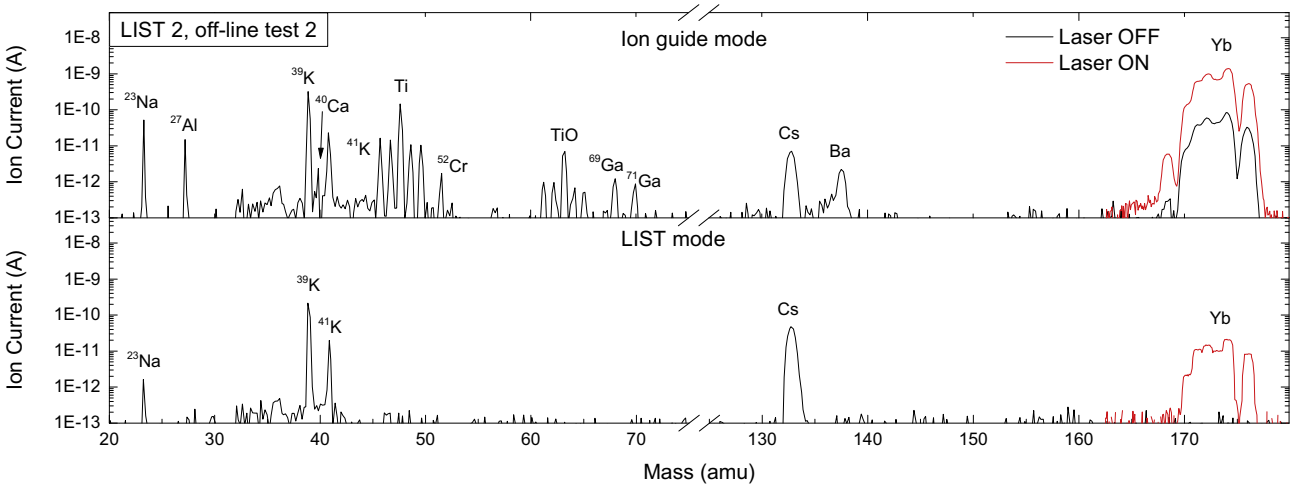

Fig. 9. Wide range mass scans taken at the off-line separator for 20 u < m < 75 u and 125 u < m < 180 u, in *ion guide mode* (upper graph) and *LIST mode* (lower graph) with LIST 2 during *off-line test 2*. Surface ionized isotopes are suppressed to the noise level of the Faraday cup, except for the alkaline elements, which are ionized by electron impact ionization behind the repeller. Laser ionized ytterbium (Yb) is visible in *LIST mode* with a LIST efficiency loss factor of ≈ 50 with respect to *ion guide mode*, as given by the red line (see color on-line).

^{40}Ca, $^{46–50}$Ti and their oxides (TiO), ^{52,53}Cr, ^{69,71}Ga, ^{133}Cs, $^{134–138}$Ba, and $^{168,\ 170–174,176}$Yb are observed as well as some unspecific, weak background in the mass region of 34 u to 45 u. In *LIST mode* only the alkaline elements sodium, potassium, cesium, and the unspecific background around 34 u to 40 u remain visible above the detection limit of the Faraday cup, while all the other species are fully suppressed. Laser resonant ionization of ytterbium enhances its contribution by about two orders of magnitude in both operation modes of the LIST, with a *LIST mode* efficiency loss factor of ~50 with respect to *ion guide mode*, as indicated in the figure by the red line (see color on-line). The insufficient suppression of the alkali metals is explained by considering alternative ionization mechanisms other than surface ionization, i.e. electron impact. Anyhow, this effect is only observed if a large deposit of these atoms has condensed on some of the cold structures downstream from the hot ion source cavity. In addition it is enhanced by the extensive outgassing of the target during the initial conditioning phase or by contamination of the structures during production and assembly. The almost complete absence of this contribution for radioactive alkaline isotopes supports this explanation as further described below. For optimizing the LIST for radioactive isotopes with low production rates, it is too time-consuming and thus rather impractical to entirely perform extended repeller scans. Instead ion count rates were measured at predetermined optimal *ion guide* and *LIST mode* repeller voltage settings. For determination of these values a repeller scan on surface ionized stable ^{48}Ti was measured under on-line conditions during *on-line run 1*, as given in Fig. 10. It shows a significantly different behavior to expectation for positive repeller potentials, i.e. *LIST mode*. As expected, an *LSF* of 4400 was determined for low repeller voltages, while a strong increase in the ion current by more than one order of magnitude was observed for further increasing positive repeller

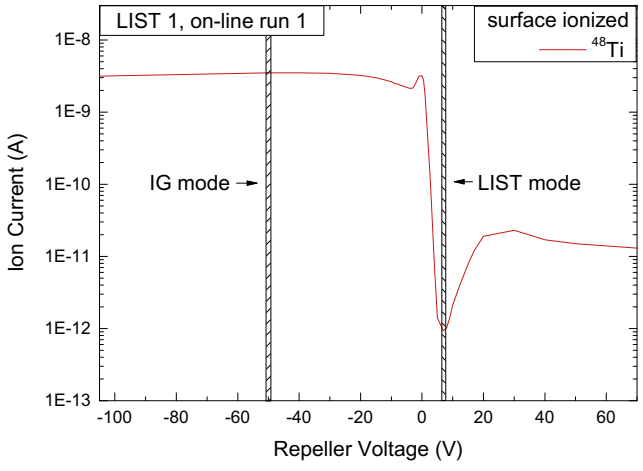

Fig. 10. Surface ionized ^{48}Ti ion current as a function of the repeller voltage measured under on-line conditions at ISOLDE with LIST 1 during *on-line run 1*. A suppression of 4400 is observed in *LIST mode* (U_{rep} ≈ 8 V) with a strong increase of interfering contamination for higher positive repeller potential.

Table 1
Ion intensities in *ion guide mode* (I_{IG}) and *LIST mode* (I_{LIST}) and LIST suppression factors (*LSF*) of several stable and radioactive isotopes obtained at the ISOLDE off-line and on-line separator. Half-lives of radioactive isotopes are given in brackets. ^{21,23,26}Na were measured with the tape station, while the stable isotopes were measured with a Faraday cup. The results for the *on-line run 2* with LIST 2 were discussed in [25] but are shown for completeness: Sodium and potassium were measured with the tape station, ^{212}Fr was measured with a Faraday cup, and ^{205,212}Fr were measured with the IKS Leuven Windmill α-detector [33]. If the ion intensity was below the background level of the Faraday cup, the tape station or the Windmill detector, the background was subtracted and a conservative value of the LIST ion intensity (given in brackets) was estimated from the background fluctuations or the statistical uncertainty, respectively.

Off-line	I_{IG}	I_{LIST}	Unit	*LSF*
LIST 1				
^{23}Na	75	0.4	pA	⩾ 230
^{48}Ti	145	0.08	pA	⩾ 1800
^{174}Yb	31	0.08	pA	⩾ 380
On-line LIST 1				
^{21}Na$_{(22.5\ s)}$	$1.6 \cdot 10^5$	100(10)	counts/μC	⩾ 16000
^{23}Na$_{(\ stable)}$	85	0.4(1)	pA	⩾ 280
^{26}Na$_{(1.07\ s)}$	$3.9 \cdot 10^4$	100(10)	counts/μC	⩾ 3900
^{39}K$_{(\ stable)}$	410	2.0(1)	pA	⩾ 230
^{48}Ti$_{(\ stable)}$	3500	0.9(1)	pA	⩾ 4400
LIST 2 [25]				
^{26}Na$_{(1.07\ s)}$	$7.5 \cdot 10^4$	50(7)	counts/μC	⩾ 10700
^{30}Na$_{(48\ ms)}$	1437	125(11)	counts/μC	⩾ 130
^{46}K$_{(105\ s)}$	$1.3 \cdot 10^4$	50(7)	counts/μC	⩾ 1850
^{205}Fr$_{(3.97\ s)}$	63520	25	counts	2540
^{212}Fr$_{(20.0\ min)}$	80	1.15	pA	70
^{220}Fr$_{(27.4\ s)}$	15379	412(20)	counts	⩾ 770

Table 2
Ion intensities in *ion guide mode* (I_{IG}) and *LIST mode* (I_{LIST}) and LIST loss factors (*LLF*) of stable and radioactive isotopes. Half-lives are given in brackets. Stable isotopes were measured with a Faraday cups (0.08 pA background) and radioactive isotopes were measured by the tape station (100 counts/μC background). The results for the *on-line run 2* are shown for completeness [25]: magnesium was measured by the tape station and polonium was measured by a Faraday cup.

Off-line	I_{IG}	I_{LIST}	Unit	*LLF*
$^{174}Yb_{(\text{stable})}$	1280	25	pA	51
On-line				
LIST 1				
$^{24}Mg_{(\text{stable})}$	250	4.9	pA	51
$^{27}Mg_{(9.46\ \text{min})}$	$2.5 \cdot 10^6$	$4.5 \cdot 10^4$	counts/μC	56
LIST 2 [25]				
$^{30}Mg_{(335\ \text{ms})}$	$8 \cdot 10^4$	4000	counts/μC	20
$^{208}Po_{(2.898\ \text{y})}$	3	0.3	pA	10

potential. This situation of strongly diminishing the LIST selectivity, is ascribed to the bad vacuum conditions related to the strong outgassing on-line target and strong electron impact ionization in this regime within the LIST structure. The choice of a low repeller potential around $U_{rep} = +7$ V for *LIST mode* and corresponding low electron acceleration avoids this effect.

An overview of the measured suppression factors under different experimental conditions is given in Table 1. Here, either the background fluctuations of the Faraday cup of ±0.1 pA or the statistical uncertainty $\sqrt{N}$ of the ion counts was taken as an upper limit for the *LIST mode* and background ion count rate, depending on the detector in use. For the stable isotopes of the alkaline elements sodium (Na) and potassium (K) the measured suppression factor was particularly and unusually low, in contrast to the radioisotopes of these elements as well as to the stable isotopes of titanium. This finding is ascribed to alternative ionization processes for all elements with particularly low ionization energy such as the alkalines, as has been pointed out above. The low LIST suppression factor obtained for stable ytterbium is limited by a too low overall ion current in *LIST mode* below the detection limit of the Faraday cup and thus represents only a lower limit. In a further test, the influence on the two radioactive isotopes of sodium with mass numbers $A = 21$ and $A = 26$ was studied, which could contaminate a desired magnesium ion beam in this mass range. The suppression of ^{21,26}Na was determined with the β-detector of the ISOLDE tape station. A LIST suppression factor of more than 1000 was observed for both.

The results of the *on-line run 2* were discussed in detail in [25]. In summary, the surface-ion suppression of LIST 2 is similar to that of LIST 1, exemplified by the results for ^{26}Na. This demonstrates that the small changes to the LIST 2 did not affect the LIST performance negatively. However, for the on-line test of LIST 2, the suppression factor for several isotopes as ^{212}Fr is poor, whilst for other isotopes of the same element, such as ^{220}Fr the suppression factor remains high. This isotope-dependent effect is explained by radioactive decay of neutral atoms that pass undisturbed through the repeller potential and condense on the relatively cold structures of the LIST. A fraction of the recoiling decay products of these atoms are captured inside the LIST to form a portion of the extracted ion beam. For a further discussion of these additional ionization mechanisms inside the LIST, we refer to our publications [25,30].

LIST efficiency loss factors *LLF* were measured for stable ^{174}Yb at the off-line separator and for different stable and radioactive magnesium isotopes on-line. The results of *on-line run 1* amount to a typical reduction factor of 50, as visible e.g. in the repeller scan of Fig. 6 for ^{174}Yb, or in the mass scans shown in Fig. 9. During *on-line run 2* a reduced LIST loss factor of only 10 in the case of polonium to 20 in the case of magnesium was observed [25]. Comparing these results to the LIST loss factor of LIST 1 with magnesium leads to an overall improvement of the laser ionization efficiency in LIST mode of a factor 2.5. The improvements are ascribed to the reduced distance of LIST 2 to the hot cavity and the corresponding better overlap of the lasers with the atomic beam entering the LIST as discussed in the previous section. All data measured are compiled in Table 2.

3.7. Absolute laser ionization efficiency

During the *off-line test 1* the absolute laser ionization efficiency in *LIST mode* was determined using a calibrated mass marker of $6.9 \cdot 10^{14}$ atoms of natural ytterbium. Taking into account the natural abundance of 31.8% of ^{174}Yb, this corresponds to $2.2 \cdot 10^{14}$ atoms on this mass. Fig. 11 shows the development of the ^{174}Yb ion current in *LIST mode* during the efficiency measurement as a function of time. The atoms were evaporated during a period of approximately 4 h by a stepwise increase of the mass marker temperature while the ion source cavity was kept at an optimum temperature. The steps and spikes in the data-set correspond to occasionally blocking of the lasers for background determination as well as to the switching from *LIST* to *ion guide mode* for verification of the stability of the LIST performance during the measurement.

A quantitative value for the LIST overall ionization efficiency was estimated by interpolating the ion current with an exponential

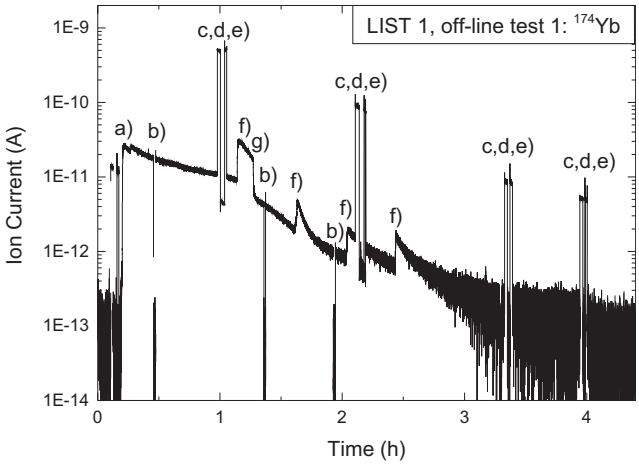

Fig. 11. Ytterbium ion current of an ytterbium-sample that was fully exhausted during 4 h at the off-line separator (*off-line run 1*) with LIST 1 for an efficiency measurement. The steps visible in the trace are due to the following actions: (a) initial temperature increase of mass marker, (b) laser blocking for Faraday cup background determination, (c) switching to ion-guide mode for comparison, (d) laser blocking in ion guide mode for surface ion background determination, (e) return to LIST mode, (f) mass marker temperature increase and (g) intentional mass marker temperature decrease for test of reproducibility. These procedures were repeated as indicated in the figure.

function over those periods, when the LIST was in *ion guide mode* or when the lasers were blocked for background measurements. The integral of the interpolated ion signal amounted to $4.4 \cdot 10^{11}$ atoms of ^{174}Yb. This corresponds to a laser ionization efficiency in *LIST mode* of $\epsilon_{\mathrm{LIST\ 1}} = 0.2\%$. This value is about twice as high as obtained in previous studies on gallium at an off-line separator [24]. Multiplying with the LIST efficiency loss factor of $LLF = 50$ as extracted from Fig. 11, the efficiency in *ion guide mode* reaches $\epsilon_{\mathrm{IG}} = 10\%$, which agrees well with the expected typical ionization efficiency obtained for standard RILIS operation [14].

For verification of this promising result, a similar procedure was applied during the *on-line run 1* for a second, independent determination of the overall LIST ionization efficiency. A calibrated sample of $2.5 \cdot 10^{16}$ atoms of stable magnesium was released from a mass marker oven into the RILIS on-line ion source cavity during a period of about 12 h. Fig. 12 shows the ^{24}Mg ion current as a function of time with the measurement performed predominantly in *ion guide mode*. Occasional measurements in *LIST mode* are visible in Fig. 12 as sharp drops in the ion signal by the LIST efficiency loss factor. The gaps in the data-set correspond to the use of the ion beam for interlaced test measurements on radioactive isotopes. To estimate the total numbers of accumulated ions, the ion current was interpolated between the periods of data taking, once again with the assumption of an exponential decline of the ion rate with time. At the beginning of the measurement, 1.5 h were required to optimize the lasers and the data acquisition system, during which data could not be taken. For this period, a conservative extrapolation of the starting ion rate was made by assuming a constant ion rate which corresponds to the first measured maximum value. In this way, a lower limit of the ionization efficiency of $\epsilon_{\mathrm{IG}} = 2.5\%$ in *ion guide* and $\epsilon_{\mathrm{LIST\ 1}} = 0.08\%$ in *LIST mode* was obtained. The optimistic estimate, indicated as dotted line in the figure, even leads to $\epsilon_{\mathrm{LIST\ 1}} = 0.25\%$ in *LIST mode*, which is in very good agreement with the LIST efficiency of ytterbium measured at the off-line separator.

In Fig. 12, a slight dependence of the efficiency loss factor on the ion current is observed with lower values for highest ion currents around 10 nA, as it was the case in the beginning of the measurement in *ion guide mode*. Here, the LIST efficiency loss factor *LLF* was significantly smaller than the typical value of about 50 as obtained later during the measurement. The observed behavior is explained by a space-charge induced reduction in the *ion guide* efficiency of these ion currents, which reach rather high values during the short duration of the laser ion pulses: the laser ion density during the peak starts to screen the penetrating extraction field of the repeller electrode as well as the guiding RF field by significant space charge effects and reduces the ion transport efficiency accordingly. This situation is not present in LIST mode, where the ion currents are much weaker. A possibility to overcome this space-charge barrier in future experiments is to operate the repeller electrode in *ion guide mode* at higher voltages than the −50 V that were used during these experiments. This has been demonstrated during *on-line run 2*, where the *ion-guide mode* extracted current of ^{235}U could be increased for high ion loads by increasing the negative voltage applied to the repeller electrode. For more details on these measurements we refer to our previous publication [25].

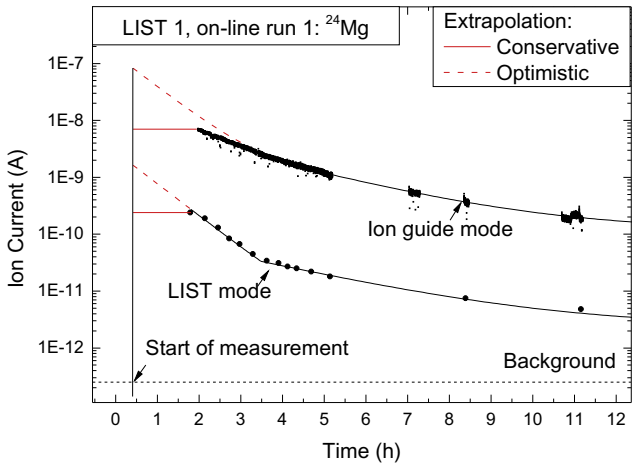

Fig. 12. On-line measurement of the laser ionization efficiency in *ion guide mode* and *LIST mode* using a 0.11 μg sample of magnesium. Data was taken with LIST 1 during *on-line run 1*. For further information see text body.

As shown in Fig. 12, an optimistic estimate of the ion guide efficiency can be obtained by extrapolating the magnesium ion current in ion guide mode by using the exponential function that was fitted to the data of LIST mode assuming that the amplitude and background signal follow the LIST loss factor of 50. This leads to an upper limit of the ion guide efficiency of $\epsilon_{\mathrm{IG}} = 12.5\%$, which is in good agreement with the results of ytterbium obtained at the off-line separator.

Taking into account the reduced LIST loss factor of only 20 obtained during the *on-line run 2*, a LIST 2 ionization efficiency of about $\epsilon_{\mathrm{LIST\ 2}} = 0.6\%$ can be assumed. However, it should be noted that the ion guide efficiency is not negatively influenced by the reduced distance of the LIST to the target.

4. Conclusion and outlook

The Laser Ion Source and Trap unit LIST has been tested and its operational status has been proven in a series of off-line and on-line measurements at the ISOLDE radioactive ion beam facility. This was the first on-line operation of such a device at a thick target ISOL facility. The results obtained on the performance of the LIST at ISOLDE are consistent with the expectations. They demonstrate that the LIST acts as an effective means of actively repelling surface ions, which often severely contaminate RILIS-ionized radioactive ion beam of the exotic species of interest.

The comparison of the measured time structures of the LIST ion bunches with ion-optical simulations led to an understanding of the origin of the different components that were observed. These results imply that the ionization efficiency increases with a reduction of the gap between the LIST and the hot cavity exit, due to the improved useful overlap between the laser beam and the effusing atom beam. This effect was demonstrated by the improvement in LIST efficiency for LIST 2.

A surface-ion suppression factor of up to four orders of magnitude was demonstrated. For few isotopes, the expected suppression factor was not achieved in the experiment. Although not yet fully understood, we believe any isotope dependent reduction in suppression must be attributed to the radioactive decay of neutral atom vapour from the hot cavity that passes the repeller potential and condenses on the relatively cold LIST structures. Future modifications to the design of the LIST will aim at reducing this source of contamination. The overall laser ionization efficiency of the LIST in *LIST mode (ion guide mode)* was determined consistently off-line for ytterbium to be $\epsilon_{\mathrm{LIST\ 1}} = 0.2\%$ ($\epsilon_{\mathrm{IG}} = 10\%$) and during the *on-line run 1* for magnesium to be at least $\epsilon_{\mathrm{LIST\ 1}} = 0.08\%$ ($\epsilon_{\mathrm{IG}} = 2.5\%$) and up to $\epsilon_{\mathrm{LIST\ 1}} = 0.25\%$ ($\epsilon_{\mathrm{IG}} = 12.5\%$), if the data was corrected for technical problems and space charge effects. For both measurements, the *ion guide mode* efficiencies agree with the expectations from the operation of the conventional ISOLDE RILIS laser ion source. The LIST efficiency loss factor amounted to typically *50* during the *on-line run 1*, but could be reduced to 20 for the *on-line run 2* by reducing the distance between the LIST and the hot cavity from 5 mm to 2.5 mm. Thus, a LIST ionization efficiency of about

$\epsilon_{\text{LIST 1}} = 0.6\%$ can be expected for LIST 2 that was in use during *on-line run 2*. An additional reduction of the distance between the LIST and the hot cavity may improve the laser ionization efficiency in LIST mode further.

Rapid switching from the highly efficient *ion guide mode* that closely corresponds to *normal RILIS* operation to the highly selective but less efficient *LIST mode* has been demonstrated successfully. In case of high ion-loads of about 10 nA and more inside the hot-cavity, a significant reduction of the *ion-guide mode* efficiency was observed due to space-charge effects. Since the space charge limit increases with an increasing extraction voltage, this problem can be avoided to a certain degree by operating the repeller at the maximum negative voltage. The *LIST-mode* efficiency, however, is not influenced by the hot-cavity ion load.

In conclusion, the LIST has proven its suitability as a robust device to operate under the harsh on-line conditions experienced at the ISOLDE front-end, showing no evidence of any degradation after 48 h of intense proton irradiation. Accordingly, these studies have paved the way for its application in a variety of future experiments at thick-target, hot-cavity on-line facilities, that demand highly pure radioactive ion beams for investigations of the most exotic low-yield short-lived nuclides.

Acknowledgments

We acknowledge the support of the ISOLDE Collaboration and technical teams. We also thank the institute of physics of the University of Mainz for the construction of the target and the LIST device and for the technical support. This work was supported by the Bundesministerium für Bildung und Forschung (BMBF, Germany) within the Wolfgang-Gentner fellowship programme as well as through the consecutive fundings of 06Mz9181I, 06Mz7177D and 05P12UMCIA and by the Max Planck Society, Germany.

References

[1] K. Blaum, J. Dilling, W. Nörtershäuser, Precision atomic physics techniques for nuclear physics, Phys. Scr. T152 (2013) 014017, http://dx.doi.org/10.1088/0031-8949/2013/T152/014017.

[2] R.N. Wolf, D. Beck, K. Blaum, C. Böhm, C. Borgmann, M. Breitenfeldt, N. Chamel, S. Goriely, F. Herfurth, M. Kowalska, S. Kreim, D. Lunney, V. Manea, E. Manea Ramirez, S. Naimi, D. Neidherr, M. Rosenbusch, L. Schweikhard, J. Stanja, F. Wienholtz, K. Zuber, Plumbing neutron stars to new depths with the binding energy of the exotic nuclide ^{82}Zn, Phys. Rev. Lett. 110 (2013) 041101, http://dx.doi.org/10.1103/PhysRevLett.110.041101.

[3] K.-L. Kratz, B. Pfeiffer, F.-K. Thielemann, W. Walters, Nuclear structure studies at ISOLDE and their impact on the astrophysical r-process, Hyperfine Interact. 129 (1–4) (2000) 185–221, http://dx.doi.org/10.1023/A:1012694723985.

[4] L.P. Gaffney, P.A. Butler, M. Scheck, A.B. Hayes, F. Wenander, M. Albers, B. Bastin, C. Bauer, A. Blazhev, S. Bönig, N. Bree, J. Cederkäll, T. Chupp, D. Cline, T.E. Cocolios, T. Davinson, H. De Witte, J. Diriken, T. Grahn, A. Herzan, M. Huyse, D.G. Jenkins, D.T. Joss, N. Kesteloot, J. Konki, M. Kowalczyk, T. Kröll, E. Kwan, R. Lutter, K. Moschner, P. Napiorkowski, J. Pakarinen, M. Pfeiffer, D. Radeck, P. Reiter, K. Reynders, S.V. Rigby, L.M. Robledo, M. Rudigier, S. Sambi, M. Seidlitz, B. Siebeck, T. Stora, P. Thoele, P. Van Duppen, M.J. Vermeulen, M. von Schmid, D. Voulot, N. Warr, K. Wimmer, K. Wrzosek-Lipska, C.Y. Wu, M. Zielinska, Studies of pear-shaped nuclei using accelerated radioactive beams, Nature 497 (2013) 199, http://dx.doi.org/10.1038/nature12073.

[5] J. Correia, K. Johnston, U. Wahl, Nuclear radioactive techniques applied to materials research, Rad. Chim. Acta 100 (2012) 127, http://dx.doi.org/10.1524/ract.2011.1873.

[6] R. dos Santos, L. Augusto, Z. Buehler, S. Lawson, M. Marzari, T. Stachura, C.-M. Stora, R. dos Santos, collaboration, CERN-MEDICIS (medical isotopes collected from ISOLDE): a new facility, Appl. Sci. 4 (2) (2014) 265–281, http://dx.doi.org/10.3390/app4020265.

[7] Y. Blumenfeld, T. Nilsson, P.V. Duppen, Facilities and methods for radioactive ion beam production, Phys. Scr. 2013 (2013) 014023, http://dx.doi.org/10.1088/0031-8949/2013/T152/014023.

[8] H. Ravn, B. Allardyce, On-line mass separators, in: D.A. Bromley (Ed.), Treatise on Heavy Ion Science, Plenum Press, New York, 1989.

[9] E. Kugler, The isolde facility, Hyperfine Interact. 129 (1–4) (2000) 23–42, http://dx.doi.org/10.1023/A:1012603025802.

[10] R. Kirchner, Review of ISOL target–ion-source systems, Nucl. Instr. Meth. B 204 (2003) 179, http://dx.doi.org/10.1016/S0168-583X(02)01900-6.

[11] U. Köster, O. Arndt, E. Bouquerel, V. Fedoseyev, H. Franberg, A. Joinet, C. Jost, I. Kerkines, R. Kirchner, Progress in ISOL target–ion source systems, Nucl. Instr. Meth. B 266 (19–20) (2008) 4229–4239, http://dx.doi.org/10.1016/j.nimb.2008.05.152.

[12] V. Mishin, V. Fedoseyev, H.-J. Kluge, V. Letokhov, H. Ravn, F. Scheerer, Y. Shirakabe, S. Sundell, O. Tengblad, Chemically selective laser ion-source for the CERN-ISOLDE on-line mass separator facility, Nucl. Instr. Meth. B 73 (1993) 550–560, http://dx.doi.org/10.1016/0168-583X(93)95839-W.

[13] V.N. Fedosseev, G. Huber, U. Köster, J. Lettry, V.I. Mishin, H. Ravn, V. Sebastian, The ISOLDE laser ion source for exotic nuclei, Hyperfine Interact. 127 (2000) 409–416, http://dx.doi.org/10.1023/A:1012609515865.

[14] V.N. Fedosseev, L.-E. Berg, D.V. Fedorov, D. Fink, O.J. Launila, R. Losito, B. Marsh, R.E. Rossel, S. Rothe, M.D. Seliverstov, A.M. Sjödin, K.D.A. Wendt, Upgrade of the resonance ionization laser ion source at ISOLDE on-line isotope separation facility: new lasers and new ion beams, Rev. Sci. Instr. 83 (2012) 02A903, http://dx.doi.org/10.1063/1.3662206.

[15] F. Wienholtz, D. Beck, K. Blaum, C. Borgmann, M. Breitenfeldt, R. Cakirli, S. George, F. Herfurth, J. Holt, M. Kowalska, S. Kreim, D. Lunney, V. Manea, J. Menendez, D. Neidherr, M. Rosenbusch, L. Schweikhard, A. Schwenk, J. Simonis, J. Stanja, R. Wolf, K. Zuber, Masses of exotic calcium isotopes pin down nuclear forces, Nature 498 (2013) 346, http://dx.doi.org/10.1038/nature12226.

[16] A.N. Andreyev, J. Elseviers, M. Huyse, P. Van Duppen, S. Antalic, A. Barzakh, N. Bree, T.E. Cocolios, V.F. Comas, J. Diriken, D. Fedorov, V. Fedosseev, S. Franchoo, J.A. Heredia, O. Ivanov, U. Köster, B.A. Marsh, K. Nishio, R.D. Page, N. Patronis, M. Seliverstov, I. Tsekhanovich, P. Van den Bergh, J. Van de Walle, M. Venhart, S. Vermote, M. Veselsky, C. Wagemans, T. Ichikawa, A. Iwamoto, P. Möller, A.J. Sierk, New type of asymmetric fission in proton-rich nuclei, Phys. Rev. Lett. 105 (2010) 252502, http://dx.doi.org/10.1103/PhysRevLett.105.252502.

[17] S. Rothe, A. Andreyev, S. Antalic, A. Borschevsky, L. Capponi, T. Cocolios, H.D. Witte, E. Eliav, V.F.D.V. Fedorov, D. Fink, S. Fritzsche, L. Ghys, M. Huyse, N. Imai, U. Kaldor, Y. Kudryavtsev, U. Köster, J. Lane, J. Lassen, V. Liberati, K. Lynch, B. Marsh, K. Nishio, D. Pauwels, V. Pershina, L. Popescu, T. Procter, D. Radulov, S. Raeder, M. Rajabali, E. Rapisarda, R. Rossel, K. Sandhu, M. Seliverstov, A. Sjödin, P.V. den Bergh, P.V. Duppen, M. Venhart, Y. Wakabayashi, K. Wendt, Measurement of the first ionization potential of astatine by laser ionization spectroscopy, Nat. Commun. 4 (2013) 1835, http://dx.doi.org/10.1038/ncomms2819.

[18] R. Kirchner, Progress in ion source development for on-line separators, Nucl. Instr. Meth. 186 (1981) 275–293, http://dx.doi.org/10.1016/0029-554X(81)90916-2.

[19] M. Huyse, Ionization in a hot cavity, Nucl. Instr. Meth. 215 (1983) 1–5, http://dx.doi.org/10.1016/0167-5087(83)91284-X.

[20] F. Schwellnus, R. Catherall, B. Crepieux, V. Fedosseev, B. Marsh, C. Mattolat, M. Menna, F. Österdahl, S. Raeder, T. Stora, K. Wendt, Study of low work function materials for hot cavity resonance ionization laser ion sources, Nucl. Instr. Meth. B 267 (2009) 1856–1861, http://dx.doi.org/10.1016/j.nimb.2009.02.068.

[21] K. Blaum, C. Geppert, H.-J. Kluge, M. Mukherjee, S. Schwarz, K. Wendt, A novel scheme for a highly selective laser ion source, Nucl. Instr. Meth. B 204 (2003) 331–335, http://dx.doi.org/10.1016/S0168-583X(02)01942-0.

[22] K. Wendt, K. Blaum, K. Brueck, C. Geppert, H.-J. Kluge, M. Mukherjee, G. Passler, S. Schwarz, S. Sirotzki, K. Wies, A highly selective laser ion source for bunched, low emittance beam release, Nucl. Phys. A 746 (2004) 47–53, http://dx.doi.org/10.1016/j.nuclphysa.2004.09.067.

[23] F. Schwellnus, K. Blaum, C. Geppert, T. Gottwald, H.-J. Kluge, C. Mattolat, W. Nörtershaeuser, K. Wies, K. Wendt, The laser ion source and trap (LIST): a highly selective ion source, Nucl. Instr. Meth. B 266 (2008) 4383–4836, http://dx.doi.org/10.1016/j.nimb.2008.05.065.

[24] F. Schwellnus, K. Blaum, R. Catherall, B. Crepieux, V.N. Fedosseev, T. Gottwald, H.-J. Kluge, B.A. Marsh, C. Mattolat, S. Rothe, T. Stora, K. Wendt, The laser ion source trap for highest isobaric selectivity in online exotic isotope production, Rev. Sci. Instr. 81 (2010) 02A515, http://dx.doi.org/10.1063/1.3318259.

[25] D.A. Fink, S.D. Richter, B. Bastin, K. Blaum, R. Catherall, T.E. Cocolios, D.V. Fedorov, V.N. Fedosseev, K. Flanagan, L. Ghys, A. Gottberg, N. Imai, T. Kron, N. Lecesne, K.T. Lynch, B.A. Marsh, T. Mendonca, D. Pauwels, E. Rapisarda, J. Ramos, R.E. Rossel, S. Rothe, M.D. Seliverstov, A.M. Sjödin, T. Stora, C. Van Beveren, K.D.A. Wendt, First application of the laser ion source trap (LIST) for on-line experiments at ISOLDE, Nucl. Instr. Meth. B317 (Part B (0)) (2013) 417–421, http://dx.doi.org/10.1016/j.nimb.2013.06.039.

[26] J. Lavoie, P. Bricault, J. Lassen, M. Pearson, Segmented linear radiofrequency quadrupole/laser ion source project at TRIUMF, Hyperfine Interact. 174 (1–3) (2007) 33–39, http://dx.doi.org/10.1007/s10751-007-9561-0.

[27] S. Raeder, H. Heggen, J. Lassen, F. Ames, D. Bishop, P. Bricault, P. Kunz, A. Mjs, A. Teigelhöfer, An ion guide laser ion source for isobar-suppressed rare isotope beams, Rev. Sci. Instr. 85 (3) (2014) 033309, http://dx.doi.org/10.1063/1.4868496.

[28] T. Sonoda, T.E. Cocolios, J. Gentens, M. Huyse, O. Ivanov, Y. Kudryavtsev, D. Pauwels, P. Van den Bergh, P. Van Duppen, The laser ion source trap (LIST) coupled to a gas cell catcher, Nucl. Instr. Meth. B 267 (2009) 2918–2926, http://dx.doi.org/10.1016/j.nimb.2009.06.085.

[29] M. Reponen, I. Moore, I. Pohjalainen, T. Kessler, P. Karvonen, J. Kurpeta, B. Marsh, S. Piszczek, V. Sonnenschein, J. Äystö, Gas jet studies towards an optimization of the IGISOL LIST method, NIMA 635 (2011) 24–34, http://dx.doi.org/10.1016/j.nima.2011.01.125.

[30] D.A. Fink, T.E. Cocolios, A.N. Andreyev, S. Antalic, A.E. Barzakh, B. Bastin, D.V. Fedorov, V.N. Fedosseev, K.T. Flanagan, L. Ghys, M. Huyse, N. Imai, T. Kron, N.

Lecesne, K.M. Lynch, B.A. Marsh, D. Pauwels, E. Rapisarda, S.D. Richter, R.E. Rossel, S. Rothe, M.D. Seliverstov, A.M. Sjödin, C. Van Beveren, P. Van Duppen, K.D.A. Wendt, In-source laser spectroscopy with the laser ion source and trap: first direct study of the ground-state properties of ^{217,219}Po (submitted for publication).

[31] S. Rothe, B. Marsh, C. Mattolat, V. Fedosseev, K. Wendt, A complementary laser system for ISOLDE RILIS, J. Phys. Conf. Ser. 312 (2010) 052020, http://dx.doi.org/10.1088/1742-6596/312/5/052020.

[32] R. Rossel, V. Fedosseev, B. Marsh, D. Richter, S. Rothe, K. Wendt, Data acquisition, remote control and equipment monitoring for ISOLDE RILIS, Nucl. Instr. Meth. B317 (Part B) (2013) 557–560, http://dx.doi.org/10.1016/j.nimb.2013.05.048.

[33] J. Elseviers, A.N. Andreyev, M. Huyse, P. Van Duppen, S. Antalic, A. Barzakh, N. Bree, T.E. Cocolios, V.F. Comas, J. Diriken, D. Fedorov, V.N. Fedosseev, S. Franchoo, L. Ghys, J.A. Heredia, O. Ivanov, U. Köster, B.A. Marsh, K. Nishio, R.D. Page, N. Patronis, M.D. Seliverstov, I. Tsekhanovich, P. Van den Bergh, J. Van De Walle, M. Venhart, S. Vermote, M. Veselský, C. Wagemans, β-delayed fission of 180Tl, Phys. Rev. C 88 (2013) 044321, http://dx.doi.org/10.1103/PhysRevC.88.044321.

[34] P. Dawson, Performance characteristics of an r.f.-only quadrupole, Int. J. Mass Spectrom. I. Proc. 67 (3) (1985) 267–276, http://dx.doi.org/10.1016/0168-1176(85)83022-6.

[35] E. Harting, F. Read, Electrostatic Lenses, Elsevier Scientific Pub Co., 1976.